Vietnam Journal of Mechanics, Vol. 48, No. 2 (2026), pp. 173 – 185
DOI: https://doi.org/10.15625/0866-7136/23666

A NOVEL SHEAR DEFORMATION THEORY FOR MAGNETO-ELECTRO-ELASTIC NANOPLATES

P. Phung-Van[1,*], **T. Nguyen-Thanh**[1,2], **P. T. Hung**[2], **Chien H. Thai**[3,4]

[1]*Faculty of Civil Engineering, HUTECH University, Ho Chi Minh City, Vietnam*

[2]*Faculty of Civil Engineering, Ho Chi Minh City University of Technology and Engineering (HCMUTE), Ho Chi Minh City, Vietnam*

[3]*Mechanics of Advanced Materials and Structures, Institute for Advanced Study in Technology, Ton Duc Thang University, Ho Chi Minh City, Vietnam*

[4]*Faculty of Civil Engineering, Ton Duc Thang University, Ho Chi Minh City, Vietnam*

[*]E-mail: pv.phuc86@hutech.edu.vn

Received: 23 October 2025 / Revised: 2 December 2025 / Accepted: 8 December 2025
Published online: 9 December 2025

Abstract. This study proposes an innovative and efficient theoretical model for analyzing magneto-electro-elastic (MEE) nanoplates. A novel approach, formulated using third- and fifth-order Chebyshev polynomials based on Eringen's theory and the shear deformation theory, is developed. This formulation automatically enforces the zero-shear-stress condition at the plate's top and bottom surfaces, eliminating the need for any supplementary constraints. Applying the principle of extended virtual displacement, the formulation is developed in weak form. By integrating a nonlocal isogeometric analysis, the proposed model effectively captures small-scale effects in MEE nanoplate structures. The natural frequencies of the MEE nanoplate are investigated with respect to geometric and a nonlocal parameter. Comparative numerical results verify the reliability and superior performance of the proposed theory over existing higher-order shear deformation models.

Keywords: Chebyshev polynomials, magneto-electro-elastic (MEE) materials, nonlocal effects, nanostructures, isogeometric analysis (IGA).

1. INTRODUCTION

Owing to their inherent coupled mechanical, electrical and magnetic behaviors, magneto-electro-elastic (MEE) materials have become prominent candidates for various advanced technological applications in sensors, advanced aerospace, robotics, and wearable devices, etc., (Martin et al., 2008; Von Hippel, 1950; Zheng et al., 2004). At the nanoscale, their mechanical responses become size-dependent, which classical elasticity theory cannot describe due to the absence of a characteristic material length scale. To overcome this limitation, several generalized continuum theories, such as couple stress, nonlocal, strain gradient and surface elasticity theories, have been proposed. Among these, Eringen's theory is widely used, as it accounts for scale effects by relating the stress at a point to strains across the entire domain. This theory has proved effective in modeling the buckling, vibration and static behavior of nanostructures.

Within this framework, numerous studies have addressed the mechanical behaviors of MEE nanostructures. Using analytical solutions, Ke et al. (2014) studied the free vibration of MEE rectangular nanoplates, while Jafarsadeghi-Pournaki et al. (2015) investigated circular nanoplates. The size-dependent analysis of MEE nanoplates resting on a foundation was

examined by Jamalpoor et al. (2017). Liu et al. (2013) examined the vibration of piezoelectric nanoplates using Kirchhoff plate theories. Employing the classical plate theory and the nonlocal strain gradient framework, Esen and Ozmen (2022) addressed the vibration and buckling of porous MEE nanoplates. Mohammadimehr and Rostami (2017) utilized an analytical solution to perform the structural responses of MEE nanoplates. Zur et al. (2020) adopted the sinusoidal shear deformation theory to evaluate the critical load and natural frequency of MEE nanoplates. Gholami and Ansari (2017) studied the postbuckling behavior of MEE nanoplates based on analytical methods. Moreover, Malikan and Nguyen (2018) examined the hygrothermal buckling analysis of MEE nanoplates through a one-variable plate theory. Subsequent advancements of the nonlocal strain gradient framework for MEE nanoplates were presented by Phung-Van et al. (2024), Thai, Hung, Nguyen-Xuan, and Phung-Van (2023), and Thai et al. (2024), whereas small-scale effects on MEE microplates were also discussed by Hung et al. (2023, 2023).

Despite these significant contributions, the coupling of nonlocal elasticity theory with isogeometric analysis for MEE nanostructures has yet to be addressed in the open literature. The present study aims to fill this gap by proposing a novel computational approach that integrates third- and fifth-order Chebyshev polynomials-based shear deformation theories within Eringen's nonlocal elasticity framework using an isogeometric analysis scheme for the analysis of MEE nanoplates. It is also noteworthy that the Chebyshev shear deformation theory has been previously applied to plate structures (Hung et al., 2025; Phung-Van et al., 2025; Thai et al., 2025), though without accounting for size-dependent effects. Compared with available formulations, a notable advantage of the proposed approach is that the zero-shear-stress condition on the plate's top and bottom faces is satisfied inherently, with no supplementary constraints required. Therefore, the proposed formulation not only extends the applicability of nonlocal elasticity within IGA but also introduces an innovative perspective for the accurate modeling of MEE nanostructures at small scales.

2. NONLOCAL ANALYSIS OF MEE NANOPLATES

According to the special Helmholtz averaging kernel, $L = \left(1-\xi^2\nabla^2\right)$, and Eringen's elasticity theory (Eringen, 1972), the basic equations for MEE structures are expressed as follows:

$$\begin{aligned}
&\left(1-\xi^2\nabla^2\right) t_{ij} = c_{ijkl}\varepsilon_{kl} - e_{ijk}E_k - q_{kij}H_k,\\
&\left(1-\xi^2\nabla^2\right) \bar{D}_i = e_{ikl}\varepsilon_{kl} - k_{ik}E_k - d_{ik}H_k,\\
&\left(1-\xi^2\nabla^2\right) \bar{B}_i = q_{ikl}\varepsilon_{kl} - d_{ik}E_k - \mu_{ik}H_k,\\
&\left(1-\xi^2\nabla^2\right) t_{ij} = \sigma_{ij}, \quad \left(1-\xi^2\nabla^2\right) \bar{D}_i = D_i, \quad \left(1-\xi^2\nabla^2\right) \bar{B}_i = B_i,\\
&\sigma_{ij,j} = \left(1-\xi^2\nabla^2\right) \rho\ddot{u}_i, \quad B_{i,i} = 0, \quad D_{i,i} = 0,
\end{aligned} \tag{1}$$

where ξ is the scale parameter for the size effect; σ_{ij}, D_i and B_i represent the local stress, electric displacement, and magnetic induction components, respectively; t_{ij}, $\bar{D}_i$, and $\bar{B}_i$ are the nonlocal stress, electric displacement, and magnetic induction components, respectively; ρ and u_i are the mass density and displacement components, respectively; $c_{ij}, e_{ij}, q_{ij}, k_{ij}, d_{ij}, \mu_{ij}$ are the piezoelectric, piezo-magnetic, dielectric permittivity, electromagnetic, and magnetic permittivity coefficients, respectively; ε_{ij}, E_i and H_i represent the strain, electric potential, and magnetic potential components, respectively.

Based on the principle of extended virtual displacements, the equations of motion for the MEE structures are obtained as follows:

$$\int_V \sigma_{ij,j}\delta u_i \mathrm{d}V + \int_V D_{i,i}\delta\Phi_i \mathrm{d}V + \int_V B_{i,i}\delta\Psi_i \mathrm{d}V + \int_V \left(1-\xi^2\nabla^2\right)\rho\ddot{u}_i\delta u_i \mathrm{d}V = 0, \tag{2}$$

where $\delta\Psi_i$, $\delta\Phi_i$ and δu_i are the virtual magnetic potential, electric potential, and displacement, respectively.

Applying the divergence theorem while omitting the Neumann boundary tractions yields

$$\int_V \delta(\varepsilon_{ij})^T \sigma_{ij} \mathrm{d}V - \int_V \delta(\mathrm{E}_i)^T D_i \mathrm{d}V - \int_V \delta(\mathrm{H}_i)^T B_i \mathrm{d}V + \int_V \left(1 - \xi^2 \nabla^2\right) \delta(u_i)^T \rho \ddot{u}_i \mathrm{d}V = 0, \quad (3)$$

where $\delta u_{i,j} = \delta\varepsilon_{ij}$; $\delta\Phi_{i,i} = -\delta \mathrm{E}_i$; $\delta\Phi_{i,i} = -\delta \mathrm{E}_i$.

Eq. (3) can be rewritten in compact form as

$$\delta U + \delta K = 0, \quad (4)$$

where

$$\begin{aligned} \delta U &= \int_V \delta(\varepsilon_{ij})^T \sigma_{ij} \mathrm{d}V - \int_V \delta(\mathrm{E}_i)^T D_i \mathrm{d}V - \int_V \delta(\mathrm{H}_i)^T B_i \mathrm{d}V, \\ \delta K &= \int_V \left(1 - \xi^2 \nabla^2\right) \delta(u_i)^T \rho \ddot{u}_i \mathrm{d}V, \end{aligned} \quad (5)$$

in which δU and δK are the virtual strain energy and virtual kinetic energy, respectively.

3. DISPLACEMENT FIELDS

According to Reddy (1984), the displacement fields are given as

$$\begin{Bmatrix} \bar{u} \\ \bar{v} \\ \bar{w} \end{Bmatrix} = \begin{Bmatrix} u_0 \\ v_0 \\ w \end{Bmatrix} - z \begin{Bmatrix} \beta_x \\ \beta_y \\ 0 \end{Bmatrix} + f(z) \begin{Bmatrix} \theta_x \\ \theta_y \\ 0 \end{Bmatrix}, \quad (6)$$

where θ_x and θ_y represent the rotations; u, v and w are the displacement components; $\beta_x = w_{,x}$ and $\beta_y = w_{,y}$; $f(z)$ is known as the transverse shear function, which defines the distribution of shear stresses across the thickness, assuming that the top and bottom surfaces are free of shear stress. In the present work, a unified formula (Hung et al., 2025; Phung-Van et al., 2025; Thai et al., 2025) is employed, in which Chebyshev polynomials of various orders are utilized, as detailed in Table 1, where the parameter p denotes the polynomial order. Fig. 1 shows the Chebyshev polynomial and its derivative. It can be observed that the zero-shear-stress requirement on the plate's top and bottom faces is inherently fulfilled within the proposed formulation without the introduction of extra conditions.

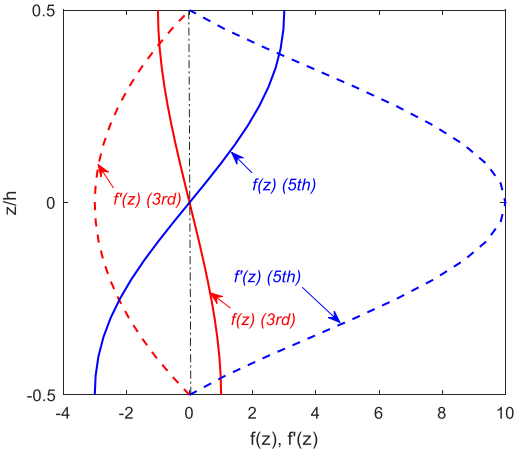

Fig. 1. Chebyshev polynomial and its derivative

Based on Eq. (6), the strains can be written as

$$\boldsymbol{\gamma} = \{\gamma_{xz} \;\; \gamma_{yz}\}^T = \boldsymbol{\varepsilon}_{s0} + f'(z)\boldsymbol{\varepsilon}_{s1}, \qquad \boldsymbol{\varepsilon} = \{\varepsilon_x \;\; \varepsilon_y \;\; \gamma_{xy}\}^T = \boldsymbol{\varepsilon}_{b0} + z\boldsymbol{\varepsilon}_{b1} + f(z)\boldsymbol{\varepsilon}_{b2}, \quad (7)$$

where $f'(z)$ is the derivative of $f(z)$ and

$$\begin{aligned} \boldsymbol{\varepsilon}_{b0} &= \begin{Bmatrix} u_{0,x} \\ v_{0,y} \\ u_{0,y} + v_{0,x} \end{Bmatrix}, \quad \boldsymbol{\varepsilon}_{b1} = -\begin{Bmatrix} \beta_{x,x} \\ \beta_{y,y} \\ \beta_{x,y} + \beta_{y,x} \end{Bmatrix}, \quad \boldsymbol{\varepsilon}_{b2} = \begin{Bmatrix} \theta_{x,x} \\ \theta_{y,y} \\ \theta_{x,y} + \theta_{y,x} \end{Bmatrix}, \\ \boldsymbol{\varepsilon}_{s0} &= \begin{Bmatrix} w_{,x} - \beta_x \\ w_{,y} - \beta_y \end{Bmatrix}, \quad \boldsymbol{\varepsilon}_{s1} = \begin{Bmatrix} \theta_x \\ \theta_y \end{Bmatrix}. \end{aligned} \quad (8)$$

Table 1. The Chebyshev function

$p = 3$ (3rd)	$f(z) = \cos\left(3\cos^{-1}\left(\frac{z}{h}\right)\right)$
$p = 5$ (5th)	$f(z) = \cos\left(5\cos^{-1}\left(\frac{z}{h}\right)\right) + \frac{5}{h}z$

The present formulation employs electric and magnetic potentials consistent with those in Ke et al. (2014)

$$\begin{aligned}\Phi(x,y,z,t) &= -\cos\left(\frac{\pi z}{h}\right)\varphi(x,y,t) + \frac{2z}{h}V_0,\\ \Psi(x,y,z,t) &= -\cos\left(\frac{\pi z}{h}\right)\psi(x,y,t) + \frac{2z}{h}\Omega_0,\end{aligned} \tag{9}$$

where V_0 is the electric voltage and Ω_0 is the magnetic potential.

Magnetic and electric potential components can be expressed

$$\begin{aligned}\mathbf{E} &= \begin{Bmatrix}E_x\\E_y\\E_z\end{Bmatrix} = -\begin{Bmatrix}\Phi_{,x}\\\Phi_{,y}\\\Phi_{,z}\end{Bmatrix} = -\begin{Bmatrix}-\cos\left(\frac{\pi z}{h}\right)\varphi_{,x}\\-\cos\left(\frac{\pi z}{h}\right)\varphi_{,y}\\\frac{\pi}{h}\sin\left(\frac{\pi z}{h}\right)\varphi + \frac{2V_0}{h}\end{Bmatrix},\\ \mathbf{H} &= \begin{Bmatrix}H_x\\H_y\\H_z\end{Bmatrix} = -\begin{Bmatrix}\Psi_{,x}\\\Psi_{,y}\\\Psi_{,z}\end{Bmatrix} = -\begin{Bmatrix}-\cos\left(\frac{\pi z}{h}\right)\psi_{,x}\\-\cos\left(\frac{\pi z}{h}\right)\psi_{,y}\\\frac{\pi}{h}\sin\left(\frac{\pi z}{h}\right)\psi + \frac{2\Omega_0}{h}\end{Bmatrix},\end{aligned} \tag{10}$$

where δU in Eq. (4) can be reformulated as follows

$$\begin{aligned}\delta U = &\int_\Omega \delta(\bar{\boldsymbol{\varepsilon}}_b)^T\left(\bar{\mathbf{D}}^b_{uu}\bar{\boldsymbol{\varepsilon}}_b - \bar{\mathbf{D}}^b_{ue}\bar{\mathbf{E}}_b - \bar{\mathbf{D}}^b_{um}\bar{\mathbf{H}}_b\right)\mathrm{d}\Omega + \int_\Omega \delta(\bar{\boldsymbol{\varepsilon}}_s)^T\left(\mathbf{D}^s_{uu}\bar{\boldsymbol{\varepsilon}}_s - \bar{\mathbf{D}}^s_{ue}\bar{\mathbf{E}}_s - \bar{\mathbf{D}}^s_{um}\bar{\mathbf{H}}_s\right)\mathrm{d}\Omega\\ &- \int_\Omega \delta(\bar{\mathbf{E}}_b)^T\left(\bar{\mathbf{D}}^b_{eu}\bar{\boldsymbol{\varepsilon}}_b + \bar{\mathbf{D}}^b_{ee}\bar{\mathbf{E}}_b + \bar{\mathbf{D}}^b_{em}\bar{\mathbf{H}}_b\right)\mathrm{d}\Omega - \int_\Omega \delta(\bar{\mathbf{E}}_s)^T\left(\bar{\mathbf{D}}^s_{eu}\bar{\boldsymbol{\varepsilon}}_s + \bar{\mathbf{D}}^s_{ee}\bar{\mathbf{E}}_s + \bar{\mathbf{D}}^s_{em}\bar{\mathbf{H}}_s\right)\mathrm{d}\Omega\\ &- \int_\Omega \delta(\bar{\mathbf{H}}_b)^T\left(\bar{\mathbf{D}}^b_{mu}\bar{\boldsymbol{\varepsilon}}_b + \bar{\mathbf{D}}^b_{me}\bar{\mathbf{E}}_b + \bar{\mathbf{D}}^b_{mm}\bar{\mathbf{H}}_b\right)\mathrm{d}\Omega - \int_\Omega \delta(\bar{\mathbf{H}}_s)^T\left(\bar{\mathbf{D}}^s_{mu}\bar{\boldsymbol{\varepsilon}}_s + \bar{\mathbf{D}}^s_{me}\bar{\mathbf{E}}_s + \bar{\mathbf{D}}^s_{mm}\bar{\mathbf{H}}_s\right)\mathrm{d}\Omega,\end{aligned} \tag{11}$$

where

$$\bar{\boldsymbol{\varepsilon}}_b = \begin{Bmatrix}\varepsilon_{b0}\\\varepsilon_{b1}\\\varepsilon_{b2}\end{Bmatrix},\quad \bar{\boldsymbol{\varepsilon}}_s = \begin{Bmatrix}\varepsilon_{s0}\\\varepsilon_{s1}\end{Bmatrix},\quad \bar{\mathbf{E}}_b = -\begin{Bmatrix}0\\0\\\varphi\end{Bmatrix},\quad \bar{\mathbf{E}}_s = -\begin{Bmatrix}\varphi_{,x}\\\varphi_{,y}\end{Bmatrix},\quad \bar{\mathbf{H}}_b = -\begin{Bmatrix}0\\0\\\psi\end{Bmatrix},$$

$$\bar{\mathbf{H}}_s = -\begin{Bmatrix}\psi_{,x}\\\psi_{,y}\end{Bmatrix},\quad \bar{\mathbf{D}}^b_{uu} = \begin{bmatrix}\mathbf{A}^b & \mathbf{B}^b & \mathbf{E}^b\\\mathbf{B}^b & \mathbf{D}^b & \mathbf{F}^b\\\mathbf{E}^b & \mathbf{F}^b & \mathbf{H}^b\end{bmatrix},\quad \mathbf{D}^s_{uu} = \begin{bmatrix}\mathbf{A}^s & \mathbf{B}^s\\\mathbf{B}^s & \mathbf{D}^s\end{bmatrix},$$

$$\left(\mathbf{A}^b,\mathbf{B}^b,\mathbf{D}^b,\mathbf{E}^b,\mathbf{F}^b,\mathbf{H}^b\right) = \int_{-h/2}^{h/2}\left(1,z,z^2,f(z),zf(z),f^2(z)\right)\mathbf{C}_{uub}\mathrm{d}z,$$

$$
\begin{aligned}
&(\mathbf{A}^s, \mathbf{B}^s, \mathbf{D}^s) = \int_{-h/2}^{h/2} \left(1, f'(z), f'^2(z)\right) \mathbf{C}_{uus} \mathrm{d}z,\\
&\bar{\mathbf{D}}^b_{ue} = \left\{\hat{\mathbf{C}}^0_{ueb} \quad \hat{\mathbf{C}}^1_{ueb} \quad \hat{\mathbf{C}}^2_{ueb}\right\}^T,\ \left(\hat{\mathbf{C}}^0_{ueb}, \hat{\mathbf{C}}^1_{ueb}, \hat{\mathbf{C}}^2_{ueb}\right) = -\int_{-h/2}^{h/2} \mathbf{C}_{ueb}\left(1, z, f(z)\right) \frac{\pi}{h} \sin\left(\frac{\pi z}{h}\right) \mathrm{d}z,\\
&\bar{\mathbf{D}}^b_{um} = \left\{\hat{\mathbf{C}}^0_{umb} \quad \hat{\mathbf{C}}^1_{umb} \quad \hat{\mathbf{C}}^2_{umb}\right\}^T,\ \left(\hat{\mathbf{C}}^0_{umb}, \hat{\mathbf{C}}^1_{umb}, \hat{\mathbf{C}}^2_{umb}\right) = -\int_{-h/2}^{h/2} \mathbf{C}_{umb}\left(1, z, f(z)\right) \frac{\pi}{h} \sin\left(\frac{\pi z}{h}\right) \mathrm{d}z,\\
&\bar{\mathbf{D}}^s_{ue} = \left\{\hat{\mathbf{C}}^0_{ues} \quad \hat{\mathbf{C}}^1_{ues}\right\}^T,\ \left(\hat{\mathbf{C}}^0_{ues}, \hat{\mathbf{C}}^1_{ues}\right) = -\int_{-h/2}^{h/2} \mathbf{C}_{ues}\left(1, f'(z)\right) \left(-\cos\left(\frac{\pi z}{h}\right)\right) \mathrm{d}z,\\
&\bar{\mathbf{D}}^s_{um} = \left\{\hat{\mathbf{C}}^0_{ums} \quad \hat{\mathbf{C}}^1_{ums}\right\}^T,\ \left(\hat{\mathbf{C}}^0_{ums}, \hat{\mathbf{C}}^1_{ums}\right) = -\int_{-h/2}^{h/2} \mathbf{C}_{ums}\left(1, f'(z)\right) \left(-\cos\left(\frac{\pi z}{h}\right)\right) \mathrm{d}z,\\
&\bar{\mathbf{D}}^b_{ee} = \int_{-h/2}^{h/2} \mathbf{C}_{eeb}\left(\frac{\pi}{h} \sin\left(\frac{\pi z}{h}\right)\right)^2 \mathrm{d}z,\ \bar{\mathbf{D}}^s_{ee} = \int_{-h/2}^{h/2} \mathbf{C}_{ees}\left(-\cos\left(\frac{\pi z}{h}\right)\right)^2 \mathrm{d}z,\\
&\bar{\mathbf{D}}^b_{em} = \int_{-h/2}^{h/2} \mathbf{C}_{emb}\left(\frac{\pi}{h} \sin\left(\frac{\pi z}{h}\right)\right)^2 \mathrm{d}z,\ \bar{\mathbf{D}}^s_{em} = \int_{-h/2}^{h/2} \mathbf{C}_{ems}\left(-\cos\left(\frac{\pi z}{h}\right)\right)^2 \mathrm{d}z,\\
&\bar{\mathbf{D}}^b_{mm} = \int_{-h/2}^{h/2} \mathbf{C}_{mmb}\left(\frac{\pi}{h} \sin\left(\frac{\pi z}{h}\right)\right)^2 \mathrm{d}z,\ \bar{\mathbf{D}}^s_{mm} = \int_{-h/2}^{h/2} \mathbf{C}_{mms}\left(-\cos\left(\frac{\pi z}{h}\right)\right)^2 \mathrm{d}z,\\
&\bar{\mathbf{D}}^b_{eu} = \bar{\mathbf{D}}^{bT}_{ue},\ \bar{\mathbf{D}}^s_{eu} = \bar{\mathbf{D}}^{sT}_{ue},\ \bar{\mathbf{D}}^b_{mu} = \bar{\mathbf{D}}^{bT}_{um},\ \bar{\mathbf{D}}^s_{mu} = \bar{\mathbf{D}}^{sT}_{um},\ \bar{\mathbf{D}}^b_{me} = \bar{\mathbf{D}}^{bT}_{em},\ \bar{\mathbf{D}}^s_{me} = \bar{\mathbf{D}}^{sT}_{em},
\end{aligned}
\tag{12}
$$

in which

$$
\begin{aligned}
&\mathbf{C}_{uub} = \begin{bmatrix} \bar{c}_{11} & \bar{c}_{12} & 0 \\ \bar{c}_{21} & \bar{c}_{22} & 0 \\ 0 & 0 & \bar{c}_{66} \end{bmatrix},\ \mathbf{C}_{ueb} = \begin{bmatrix} 0 & 0 & \bar{e}_{31} \\ 0 & 0 & \bar{e}_{32} \\ 0 & 0 & 0 \end{bmatrix},\ \mathbf{C}_{umb} = \begin{bmatrix} 0 & 0 & \bar{q}_{31} \\ 0 & 0 & \bar{q}_{32} \\ 0 & 0 & 0 \end{bmatrix},\ \mathbf{C}_{eeb} = \begin{bmatrix} 0 & 0 & 0 \\ 0 & 0 & 0 \\ 0 & 0 & \bar{k}_{33} \end{bmatrix},\\
&\mathbf{C}_{uus} = \begin{bmatrix} \bar{c}_{55} & 0 \\ 0 & \bar{c}_{44} \end{bmatrix},\ \mathbf{C}_{ues} = \begin{bmatrix} \bar{e}_{15} & 0 \\ 0 & \bar{e}_{24} \end{bmatrix},\ \mathbf{C}_{ums} = \begin{bmatrix} \bar{q}_{15} & 0 \\ 0 & \bar{q}_{24} \end{bmatrix},\ \mathbf{C}_{ees} = \begin{bmatrix} \bar{k}_{11} & 0 \\ 0 & \bar{k}_{22} \end{bmatrix},\\
&\mathbf{C}_{emb} = \begin{bmatrix} 0 & 0 & 0 \\ 0 & 0 & 0 \\ 0 & 0 & \bar{d}_{33} \end{bmatrix},\ \mathbf{C}_{mmb} = \begin{bmatrix} 0 & 0 & 0 \\ 0 & 0 & 0 \\ 0 & 0 & \bar{\mu}_{33} \end{bmatrix},\ \mathbf{C}_{ems} = \begin{bmatrix} \bar{d}_{11} & 0 \\ 0 & \bar{d}_{22} \end{bmatrix},\ \mathbf{C}_{mms} = \begin{bmatrix} \bar{\mu}_{11} & 0 \\ 0 & \bar{\mu}_{22}, \end{bmatrix}
\end{aligned}
\tag{13}
$$

and (Ke et al., 2014)

$$
\begin{aligned}
&\bar{c}_{11} = c_{11} - \frac{c_{13}^2}{c_{33}},\ \bar{c}_{12} = c_{12} - \frac{c_{13}^2}{c_{33}},\ \bar{c}_{66} = c_{66},\ \bar{c}_{55} = c_{55},\ \bar{c}_{44} = c_{44},\ \bar{e}_{31} = e_{31} - \frac{e_{33}c_{13}}{c_{33}},\\
&\bar{e}_{15} = e_{15},\ \bar{q}_{31} = q_{31} - \frac{q_{33}c_{13}}{c_{33}},\ \bar{q}_{15} = q_{15},\ \bar{k}_{33} = k_{33} + \frac{e_{33}^2}{c_{33}},\ \bar{k}_{11} = k_{11},\ \bar{d}_{33} = d_{33} + \frac{q_{33}e_{33}}{c_{33}},\\
&\bar{d}_{11} = d_{11},\ \bar{\mu}_{33} = \mu_{33} + \frac{q_{33}^2}{c_{33}},\ \bar{\mu}_{11} = \mu_{11},
\end{aligned}
\tag{14}
$$

δK in Eq. (4) is similarly formulated as

$$
\delta K = \int_\Omega \left(1 - \mu\nabla^2\right) \delta\bar{\mathbf{u}}^T \mathbf{I}_m \ddot{\bar{\mathbf{u}}} \mathrm{d}\Omega = \mathbf{0},
\tag{15}
$$

where

$$
\begin{aligned}
&\bar{\mathbf{u}} = \begin{Bmatrix} \mathbf{u}_0 \\ \mathbf{u}_1 \\ \mathbf{u}_2 \end{Bmatrix},\quad \mathbf{u}_0 = \begin{Bmatrix} u_0 \\ v_0 \\ w_0 \end{Bmatrix},\quad \mathbf{u}_1 = -\begin{Bmatrix} \beta_x \\ \beta_y \\ 0 \end{Bmatrix},\quad \mathbf{u}_2 = \begin{Bmatrix} \theta_x \\ \theta_y \\ 0 \end{Bmatrix},\quad \mathbf{I}_m = \begin{bmatrix} \mathbf{I}_1 & \mathbf{I}_2 & \mathbf{I}_4 \\ \mathbf{I}_2 & \mathbf{I}_3 & \mathbf{I}_5 \\ \mathbf{I}_4 & \mathbf{I}_5 & \mathbf{I}_6 \end{bmatrix},\\
&\left(\mathbf{I}_1, \mathbf{I}_2, \mathbf{I}_3, \mathbf{I}_4, \mathbf{I}_5, \mathbf{I}_6\right) = \int_{-h/2}^{h/2} \rho\left(1, z, z^2, f(z), zf(z), f^2(z)\right) \mathbf{I}_{3\times3} \mathrm{d}z,
\end{aligned}
\tag{16}
$$

where ρ is mass density.

The expression for the change in potential energy resulting from in-plane loading, including pre-buckling mechanical forces, is as follows:

$$\delta V = -h\int_{\Omega}\left(1-\xi^2\nabla^2\right)\delta\begin{Bmatrix}w_{,x}\\ w_{,y}\end{Bmatrix}^{\mathrm{T}}\begin{bmatrix}N_x^{mech}+N_x^{elec}+N_x^{mag} & 0\\ 0 & N_y^{mech}+N_y^{elec}+N_y^{mag}\end{bmatrix}\begin{Bmatrix}w_{,x}\\ w_{,y}\end{Bmatrix}\mathrm{d}\Omega, \tag{17}$$

or

$$\delta V = -h\int_{\Omega}\left(1-\xi^2\nabla^2\right)\delta\left(\mathbf{B}_g\right)^{\mathrm{T}}\begin{bmatrix}N_x^{mech}+N_x^{elec}+N_x^{mag} & 0\\ 0 & N_y^{mech}+N_y^{elec}+N_y^{mag}\end{bmatrix}\mathbf{B}_g\mathrm{d}\Omega, \tag{18}$$

where N_x^{mech} and N_y^{mech} indicate the in-plane mechanical loads, and $N_x^{elec}=N_y^{elec}=2\bar{e}_{31}V_0$; $N_x^{mag}=N_y^{mag}=2\bar{q}_{31}\Omega_0$ (Jamalpoor et al., 2017; Malikan & Nguyen, 2018).

Consequently, the equations of motion in Eq. (4) are written as

$$\delta U+\delta K-\delta V=0. \tag{19}$$

4. NURBS BASIS FUNCTIONS

Using NURBS basis functions (N_I), the displacement field in Eq. (6) is represented as follows (Hughes et al., 2005):

$$\mathbf{u}^h(x,y)=\sum_{I=1}^{m\times n}N_I(x,y)\,\mathbf{I}_{9\times 9}\mathbf{q}_I, \tag{20}$$

where $\mathbf{q}_I=\left\{u_I \quad v_I \quad w_I \quad \theta_{xI} \quad \theta_{yI} \quad \beta_{xI} \quad \beta_{yI} \quad \varphi_I \quad \psi_I\right\}^T$.

Substituting Eq. (20) into Eq. (8), we have

$$\begin{aligned}\bar{\boldsymbol{\varepsilon}}_b&=\left\{\boldsymbol{\varepsilon}_{b0} \quad \boldsymbol{\varepsilon}_{b1} \quad \boldsymbol{\varepsilon}_{b2}\right\}^T=\sum_{I=1}^{m\times n}\left\{\mathbf{B}_{b0I} \quad \mathbf{B}_{b1I} \quad \mathbf{B}_{b2I}\right\}^T\mathbf{q}_I=\sum_{I=1}^{m\times n}\bar{\mathbf{B}}_{bI}\mathbf{q}_I,\\ \bar{\boldsymbol{\varepsilon}}_s&=\left\{\boldsymbol{\varepsilon}_{s0} \quad \boldsymbol{\varepsilon}_{s1}\right\}^T=\sum_{I=1}^{m\times n}\left\{\mathbf{B}_{s0I} \quad \mathbf{B}_{s1I}\right\}^T\mathbf{q}_I=\sum_{I=1}^{m\times n}\bar{\mathbf{B}}_{sI}\mathbf{q}_I,\end{aligned} \tag{21}$$

where

$$\mathbf{B}_{b0I}=\begin{bmatrix}N_{I,x} & 0 & 0 & 0 & 0 & 0 & 0 & 0 & 0\\ 0 & N_{I,y} & 0 & 0 & 0 & 0 & 0 & 0 & 0\\ N_{I,y} & N_{I,x} & 0 & 0 & 0 & 0 & 0 & 0 & 0\end{bmatrix},\ \mathbf{B}_{b1I}=-\begin{bmatrix}0 & 0 & 0 & 0 & 0 & 0 & 0 & N_{I,x} & 0 & 0 & 0\\ 0 & 0 & 0 & 0 & 0 & 0 & 0 & 0 & N_{I,y} & 0 & 0\\ 0 & 0 & 0 & 0 & 0 & 0 & 0 & N_{I,y} & N_{I,x} & 0 & 0\end{bmatrix},$$

$$\mathbf{B}_{b2I}=\begin{bmatrix}0 & 0 & 0 & N_{I,x} & 0 & 0 & 0 & 0 & 0\\ 0 & 0 & 0 & 0 & N_{I,y} & 0 & 0 & 0 & 0\\ 0 & 0 & 0 & N_{I,y} & N_{I,x} & 0 & 0 & 0 & 0\end{bmatrix}, \tag{22}$$

$$\mathbf{B}_{s0I}=\begin{bmatrix}0 & 0 & N_{I,x} & 0 & 0 & -N_I & 0 & 0 & 0\\ 0 & 0 & N_{I,y} & 0 & 0 & 0 & -N_I & 0 & 0\end{bmatrix},\ \mathbf{B}_{s1I}=\begin{bmatrix}0 & 0 & 0 & N_I & 0 & 0 & 0 & 0 & 0\\ 0 & 0 & 0 & 0 & N_I & 0 & 0 & 0 & 0\end{bmatrix}. \tag{23}$$

Substituting Eq. (20) into Eq. (10), we obtain

$$\bar{\mathbf{E}}_b=\sum_{I=1}^{m\times n}\bar{\mathbf{B}}_{b\varphi I}\mathbf{d}_I,\quad \bar{\mathbf{E}}_s=\sum_{I=1}^{m\times n}\bar{\mathbf{B}}_{s\varphi I}\mathbf{d}_I,\quad \bar{\mathbf{H}}_b=\sum_{I=1}^{m\times n}\bar{\mathbf{B}}_{b\psi I}\mathbf{d}_I,\quad \bar{\mathbf{H}}_s=\sum_{I=1}^{m\times n}\bar{\mathbf{B}}_{s\psi I}\mathbf{d}_I, \tag{24}$$

where

$$\bar{\mathbf{B}}_{b\varphi I}=\begin{bmatrix}0&0&0&0&0&0&0&0&0\\0&0&0&0&0&0&0&0&0\\0&0&0&0&0&0&0&-N_I&0\end{bmatrix},\quad \bar{\mathbf{B}}_{s\varphi I}=\begin{bmatrix}0&0&0&0&0&0&0&-N_{I,x}&0\\0&0&0&0&0&0&0&-N_{I,y}&0\end{bmatrix},$$
$$\bar{\mathbf{B}}_{b\psi I}=\begin{bmatrix}0&0&0&0&0&0&0&0&0\\0&0&0&0&0&0&0&0&0\\0&0&0&0&0&0&0&0&-N_I\end{bmatrix},\quad \bar{\mathbf{B}}_{s\psi I}=\begin{bmatrix}0&0&0&0&0&0&0&0&-N_{I,x}\\0&0&0&0&0&0&0&0&-N_{I,y}\end{bmatrix}. \tag{25}$$

Inserting Eq. (20) into Eq. (16) yields the components of the displacement fields as follows:

$$\bar{\mathbf{u}}=\begin{Bmatrix}\mathbf{u}_0&\mathbf{u}_1&\mathbf{u}_2\end{Bmatrix}^T=\sum_{I=1}^{m\times n}\begin{Bmatrix}\mathbf{M}_{0I}&\mathbf{M}_{1I}&\mathbf{M}_{2I}\end{Bmatrix}^T\mathbf{q}_I=\sum_{I=1}^{m\times n}\bar{\mathbf{M}}_I\mathbf{q}_I, \tag{26}$$

$$\mathbf{M}_{0I}=\begin{bmatrix}N_I&0&0&0&0&0&0&0&0\\0&N_I&0&0&0&0&0&0&0\\0&0&N_I&0&0&0&0&0&0\end{bmatrix},\mathbf{M}_{1I}=-\begin{bmatrix}0&0&0&0&0&N_I&0&0&0\\0&0&0&0&0&0&N_I&0&0\\0&0&0&0&0&0&0&0&0\end{bmatrix},$$
$$\mathbf{M}_{2I}=\begin{bmatrix}0&0&0&N_I&0&0&0&0&0\\0&0&0&0&N_I&0&0&0&0\\0&0&0&0&0&0&0&0&0\end{bmatrix}. \tag{27}$$

The matrix $\mathbf{B}_g$ is represented as follows:

$$\mathbf{B}_g=\sum_{I=1}^{m\times n}\mathbf{B}_{gI}\mathbf{d}_I, \tag{28}$$

where

$$\mathbf{B}_{gI}=\begin{bmatrix}0&0&N_{I,x}&0&0&0&0&0&0\\0&0&N_{I,y}&0&0&0&0&0&0\end{bmatrix}^T. \tag{29}$$

The final equation is obtained as follows:

$$\left(\left(\mathbf{K}-\mathbf{K}_g\right)-\omega^2\mathbf{M}\right)\bar{\mathbf{q}}=0, \tag{30}$$

where $\mathbf{K}$, $\mathbf{M}$ and $\mathbf{K}_g$ are the global stiffness matrix, mass matrix, and geometry matrix formulated as follows:

$$\begin{aligned}\mathbf{K}=&\int_\Omega(\bar{\mathbf{B}}_b)^T\bar{\mathbf{D}}^b_{uu}\bar{\mathbf{B}}_b\mathrm{d}\Omega-\int_\Omega(\bar{\mathbf{B}}_b)^T\bar{\mathbf{D}}^b_{ue}\bar{\mathbf{B}}_{b\varphi}\mathrm{d}\Omega-\int_\Omega(\bar{\mathbf{B}}_b)^T\bar{\mathbf{D}}^b_{um}\bar{\mathbf{B}}_{b\psi}\mathrm{d}\Omega+\int_\Omega(\bar{\mathbf{B}}_s)^T\mathbf{D}^s_{uu}\bar{\mathbf{B}}_s\mathrm{d}\Omega\\&-\int_\Omega(\bar{\mathbf{B}}_s)^T\bar{\mathbf{D}}^s_{ue}\bar{\mathbf{B}}_{s\varphi}\mathrm{d}\Omega-\int_\Omega(\bar{\mathbf{B}}_s)^T\bar{\mathbf{D}}^s_{um}\bar{\mathbf{B}}_{s\psi}\mathrm{d}\Omega-\int_\Omega\left(\bar{\mathbf{B}}_{b\varphi}\right)^T\bar{\mathbf{D}}^b_{eu}\bar{\mathbf{B}}_b\mathrm{d}\Omega-\int_\Omega\left(\bar{\mathbf{B}}_{b\varphi}\right)^T\bar{\mathbf{D}}^b_{ee}\bar{\mathbf{B}}_{b\varphi}\mathrm{d}\Omega\\&-\int_\Omega\left(\bar{\mathbf{B}}_{b\varphi}\right)^T\bar{\mathbf{D}}^b_{em}\bar{\mathbf{B}}_{b\psi}\mathrm{d}\Omega-\int_\Omega\left(\bar{\mathbf{B}}_{s\varphi}\right)^T\bar{\mathbf{D}}^s_{eu}\bar{\mathbf{B}}_s\mathrm{d}\Omega-\int_\Omega\left(\bar{\mathbf{B}}_{s\varphi}\right)^T\bar{\mathbf{D}}^s_{ee}\bar{\mathbf{B}}_{s\varphi}\mathrm{d}\Omega-\int_\Omega\left(\bar{\mathbf{B}}_{s\varphi}\right)^T\bar{\mathbf{D}}^s_{em}\bar{\mathbf{B}}_{s\psi}\mathrm{d}\Omega\\&-\int_\Omega\left(\bar{\mathbf{B}}_{b\psi}\right)^T\bar{\mathbf{D}}^b_{mu}\bar{\mathbf{B}}_b\mathrm{d}\Omega-\int_\Omega\left(\bar{\mathbf{B}}_{b\psi}\right)^T\bar{\mathbf{D}}^b_{me}\bar{\mathbf{B}}_{b\varphi}\mathrm{d}\Omega-\int_\Omega\left(\bar{\mathbf{B}}_{b\psi}\right)^T\bar{\mathbf{D}}^b_{mm}\bar{\mathbf{B}}_{b\psi}\mathrm{d}\Omega-\int_\Omega\left(\bar{\mathbf{B}}_{s\psi}\right)^T\bar{\mathbf{D}}^s_{mu}\bar{\mathbf{B}}_s\mathrm{d}\Omega\\&-\int_\Omega\left(\bar{\mathbf{B}}_{s\psi}\right)^T\bar{\mathbf{D}}^s_{me}\bar{\mathbf{B}}_{s\varphi}\mathrm{d}\Omega-\int_\Omega\left(\bar{\mathbf{B}}_{s\psi}\right)^T\bar{\mathbf{D}}^s_{mm}\bar{\mathbf{B}}_{s\psi}\mathrm{d}\Omega,\\\mathbf{K}_g=&\int_\Omega\left(1-\xi^2\nabla^2\right)\left(\mathbf{B}_g\right)^T\begin{bmatrix}N^{elec}_x+N^{mag}_x&0\\0&N^{elec}_y+N^{mag}_y\end{bmatrix}\mathbf{B}_g\mathrm{d}\Omega,\\\mathbf{M}=&\int_\Omega\left(1-\xi^2\nabla^2\right)\bar{\mathbf{M}}^T\mathbf{I}_m\bar{\mathbf{M}}\mathrm{d}\Omega,\end{aligned} \tag{31}$$

in which ω and $\bar{\mathbf{q}}$ are the natural frequency and mode shape, respectively.

5. NUMERICAL EXAMPLES

This section considers a MEE nanoplate made of $BaTi_2O_3$ and $CoFe_2O_4$. Table 2 provides the corresponding material properties. Two MEE models including square and circular nanoplates, as shown in Fig. 2, are performed. The non-dimensional frequency is subsequently examined and derived as follows:

$$\text{+ Square nanoplate} \qquad \bar{\omega} = \omega L\sqrt{\rho/c_{11e}}, \tag{32}$$

$$\text{+ Circle nanoplates} \qquad \bar{\omega} = \omega\frac{R^2}{h}\sqrt{\rho/c_{11e}}. \tag{33}$$

Table 2. Material properties of $BaTi_2O_3$-$CoFe_2O_4$

Elastic (GPa)	$c_{11} = c_{22} = 226; c_{12} = 125; c_{13} = 124; c_{44} = c_{55} = 44.2; c_{66} = 50.5$
Piezoelectric (C/m^2)	$e_{31} = e_{32} = -2.2; e_{33} = 9.3; e_{15} = 5.8$
Dielectric (10^{-9} C/V.m)	$k_{11} = k_{22} = 5.64; k_{33} = 6.35$
Piezomagnetic (N/A.m)	$q_{15} = q_{24} = 275; q_{31} = q_{32} = 290.1; q_{33} = 349.9$
Magnetoelectric (10^{-12} Ns/VC)	$d_{11} = d_{22} = 5.367; d_{33} = 2737.5$
Magnetic (10^{-6} Ns^2/C^2)	$\mu_{11} = \mu_{22} = -297; \mu_{33} = 83.5$

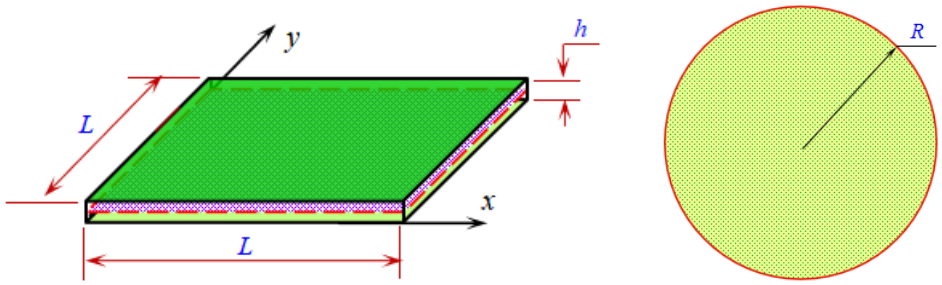

(a) A square nanoplate (b) A circle nanoplate

Fig. 2. MEE nanoplate models

5.1. A square MEE nanoplate

Considering a simply supported square MEE plate with a length (L) and thickness (h), the influence of $e_0 = \xi/L$ on the lowest two fundamental vibration modes of the MEE nanoplate with $L = 60$, $L/h = 15$ is summarized in Table 3. The numerical outcomes obtained in this study are verified with those reported by Ke et al. (2014) employing the Kirchhoff plate theory, by Gholami et al. (2017) using HSDT, and by Thai, Ferreira, et al. (2023) through isogeometric analysis. Overall, the results in Table 3 show excellent agreement with the analytical solutions (Ke et al., 2014), the Navier's solution approach (Gholami et al., 2017), and the numerical method (Thai, Ferreira, et al., 2023), demonstrating the reliability of the proposed approach. The results further show that larger values of the nonlocal parameter lead to lower natural frequencies, indicating a softening effect on the structural stiffness.

Subsequently, the first five natural frequencies of the MEE nanoplate with $L/h = 10$ and 100 are analyzed, with the outcomes presented in Table 4. The results once again reveal an excellent correspondence with those available in the literature. In addition, it is evident that as the length-to-thickness ratio decreases, the corresponding frequencies rise, indicating a stiffening behavior in thicker plates.

Table 3. The lowest two frequencies of the MEE nanoplates $(L = 60, L/h = 15)$

Method	$e_0 = 0$		$e_0 = 0.2$		$e_0 = 0.4$	
	Mode 1	Mode 2	Mode 1	Mode 2	Mode 1	Mode 2
Thai, Ferreira, et al. (2023)	0.3830	0.9329	0.2863	0.0541	0.1878	0.3128
Gholami et al. (2017)	0.3682	0.9136	0.2753	0.5372	0.1806	0.3103
Ke et al. (2014)	0.3698	0.9247	0.2764	0.5362	0.1813	0.3100
Present $(p = 3)$	0.3830	0.9329	0.2863	0.5410	0.1878	0.3128
Present $(p = 5)$	0.3830	0.9330	0.2863	0.5410	0.1878	0.3128

Table 4. Effects of the length-to-thickness ratio on the first five frequencies of the MEE nanoplate

L/h	e_0	Method	Mode				
			1	2	3	4	5
100	1	Thai, Ferreira, et al. (2023)	0.0128	0.0206	0.0206	0.0261	0.0293
		Present $(p = 3)$	0.0128	0.0206	0.0206	0.0261	0.0293
		Present $(p = 5)$	0.0128	0.0206	0.0206	0.0261	0.0293
	0.5	Thai, Ferreira, et al. (2023)	0.0240	0.0400	0.0400	0.5130	0.0578
		Present $(p = 3)$	0.0240	0.0400	0.0400	0.0513	0.0578
		Present $(p = 5)$	0.0240	0.040	0.0400	0.0513	0.0578
10	1	Thai, Ferreira, et al. (2023)	0.1234	0.1878	0.1878	0.2275	0.2476
		Present $(p = 3)$	0.1234	0.1878	0.1878	0.2275	0.2476
		Present $(p = 5)$	0.1234	0.1878	0.1878	0.2276	0.2477
	0.5	Thai, Ferreira, et al. (2023)	0.2307	0.3649	0.3649	0.4468	0.4879
		Present $(p = 3)$	0.2307	0.3649	0.3649	0.4468	0.4879
		Present $(p = 5)$	0.2308	0.3649	0.3649	0.4469	0.4881

Finally, the mode shapes associated with the six lowest vibration modes are depicted in Fig. 3. These shapes are consistent with the expected physical deformation patterns of the nanoplate, further validating the accuracy of the current numerical model.

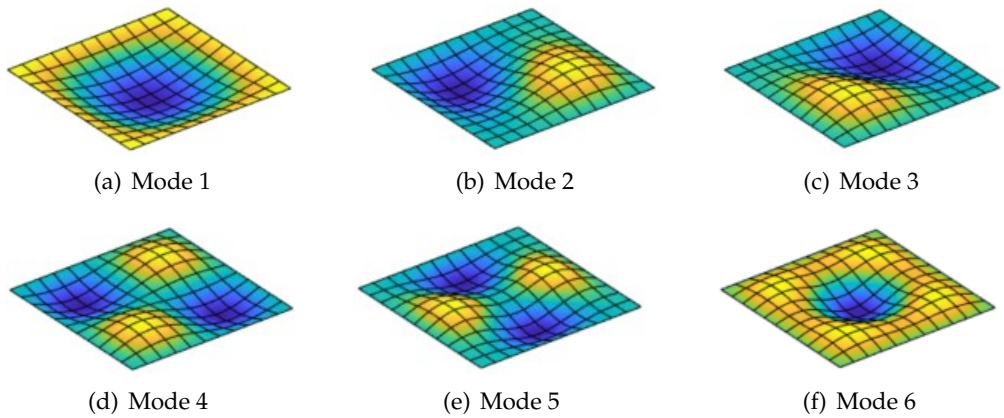

(a) Mode 1 (b) Mode 2 (c) Mode 3

(d) Mode 4 (e) Mode 5 (f) Mode 6

Fig. 3. The lowest six mode shapes of the MEE nanoplates with $L/h = 10$ and $e_0 = 0.5$

5.2. A circular MEE nanoplate

For MEE circular nanoplates with a radius R, the non-dimensional natural frequency is formulated in Eq. (33). The first natural frequency of a clamped MEE circular nanoplate is computed, and the results are provided in Table 5. The data show that a larger nonlocal parameter reduces the frequency, reflecting a decrease in the effective stiffness. Conversely, increasing the radius-to-thickness ratio results in higher natural frequencies.

Table 5. The first six frequencies of the clamped MEE circular nanoplate with $R = 10$

R/h	ξ	Method	Mode					
			1	2	3	4	5	6
10	1	Present $(p = 3)$	2.8271	5.4692	5.4692	8.2828	8.2828	9.2384
		Present $(p = 5)$	2.8273	5.4699	5.4699	8.2844	8.2860	9.2403
	2	Present $(p = 3)$	2.5881	4.5767	4.5767	6.3978	6.3991	7.0073
		Present $(p = 5)$	2.5883	4.5773	4.5773	6.3990	6.4002	7.0086
	3	Present $(p = 3)$	2.2948	3.7328	3.7328	4.9417	4.9417	5.3691
		Present $(p = 5)$	2.2950	3.7333	3.7333	4.9426	4.9436	5.3701
50	1	Present $(p = 3)$	2.9211	5.8138	5.8138	9.0562	9.0904	10.2078
		Present $(p = 5)$	2.9211	5.8138	5.8138	9.0562	9.0905	10.2079
	2	Present $(p = 3)$	2.6720	4.8553	4.8553	6.9754	7.0065	7.7267
		Present $(p = 5)$	2.6720	4.8553	4.8553	6.9754	7.0066	7.7268
	3	Present $(p = 3)$	2.3675	3.9550	3.9550	5.3805	5.4073	5.9178
		Present $(p = 5)$	2.3676	3.9551	3.9551	5.3806	5.4074	5.9178

Subsequently, the effects of both the applied electric voltage and magnetic potential on the fundamental frequency of the clamped MEE circular nanoplate with $(p = 5)$ are investigated, as presented in Fig. 4. The results reveal opposite trends: the frequency rises as the electric voltage increases, whereas it declines when the magnetic potential becomes stronger. These trends imply that an elevated electric voltage enhances the effective stiffness of the plate, while a higher magnetic potential reduces it.

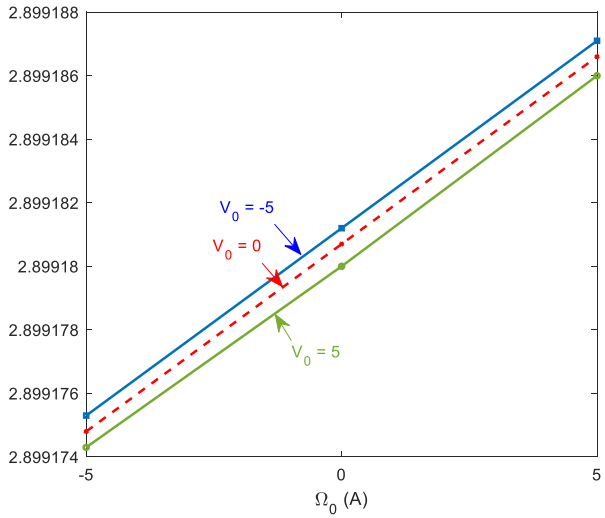

Fig. 4. Effects of the magnetic potential and external electric voltage on the first frequency of the clamped MEE circular nanoplate $(R = 10, R/h = 20, \xi)$

6. CONCLUSIONS

This study presented a novel theoretical framework for MEE nanoplates by combining Eringen's theory, the Chebyshev shear deformation theory, and isogeometric analysis. The formulation, derived through the principle of extended virtual displacements, successfully incorporates small-scale effects while maintaining computational efficiency and accuracy. Besides, this formulation automatically enforces the zero-shear-stress condition at the plate's top and bottom surfaces, eliminating the need for any supplementary constraints. The numerical investigations demonstrate excellent agreement with reference results, confirming the reliability and robustness of the proposed model. Parametric studies reveal that increasing the nonlocal parameter leads to a noticeable reduction in natural frequencies, highlighting the softening influence of nonlocal effects on the structural stiffness of nanoplates. Conversely, decreasing the length-to-thickness ratio produces higher frequencies, indicating enhanced stiffness in thicker plates. Moreover, applying an electric voltage effectively enhances the plate stiffness, whereas increasing the magnetic potential reduces it. Overall, the proposed nonlocal Chebyshev–IGA formulation provides an accurate, efficient, and versatile tool for the calculation and simulation of MEE nanostructures, advanced nano-scale devices, and smart material systems.

DECLARATION OF COMPETING INTEREST

The authors declare that they have no known competing financial interests or personal relationships that could have appeared to influence the work reported in this paper.

CREDIT AUTHOR STATEMENT

P. Phung-Van: *Conceptualization, Methodology, Formal analysis, Investigation, Visualization, Writing – original draft*. T. Nguyen-Thanh: *Software, Validation, Investigation, Writing – review & editing*. P. T. Hung: *Software, Investigation, Visualization, Writing – review & editing*. Chien H. Thai: *Validation, Visualization, Writing – review & editing*.

FUNDING

This research is funded by Vietnam National Foundation for Science and Technology Development (NAFOSTED) under grant number 107.02-2023.79.

REFERENCES

Eringen, A. C. (1972). Nonlocal polar elastic continua. *International Journal of Engineering Science*, *10*(1), 1–16. https://doi.org/10.1016/0020-7225(72)90070-5

Esen, I., & Ozmen, R. (2022). Thermal vibration and buckling of magneto-electro-elastic functionally graded porous nanoplates using nonlocal strain gradient elasticity. *Composite Structures*, *296*, 115878. https://doi.org/10.1016/j.compstruct.2022.115878

Gholami, R., & Ansari, R. (2017). A unified nonlocal nonlinear higher-order shear deformable plate model for postbuckling analysis of piezoelectric-piezomagnetic rectangular nanoplates with various edge supports. *Composite Structures*, *166*, 202–218. https://doi.org/10.1016/j.compstruct.2017.01.045

Gholami, R., Ansari, R., & Gholami, Y. (2017). Size-dependent bending, buckling and vibration of higher-order shear deformable magneto-electro-thermo-elastic rectangular nanoplates. *Materials Research Express*, *4*(6), 065702. https://doi.org/10.1088/2053-1591/aa711c

Hughes, T. J. R., Cottrell, J. A., & Bazilevs, Y. (2005). Isogeometric analysis: CAD, finite elements, NURBS, exact geometry and mesh refinement. *Computer Methods in Applied Mechanics and Engineering*, *194*(39–41), 4135–4195. https://doi.org/10.1016/j.cma.2004.10.008

Hung, P. T., Phung-Van, P., & Thai, C. H. (2023). Small scale thermal analysis of piezoelectric–piezomagnetic fg microplates using modified strain gradient theory. *International Journal of Mechanics and Materials in Design*, *19*(4), 739–761. https://doi.org/10.1007/s10999-023-09651-y

Hung, P., Thai, C. H., & Phung-Van, P. (2023). Isogeometric bending and free vibration analyses of carbon nanotube-reinforced magneto-electric-elastic microplates using a four variable refined plate theory. *Computers & Structures*, *287*, 107121. https://doi.org/10.1016/j.compstruc.2023.107121

Hung, P., Thai, C. H., & Phung-Van, P. (2025). A novel meshfree method for free vibration behavior of the functionally graded carbon nanotube-reinforced composite plates using a new shear deformation theory. *Computers & Mathematics with Applications*, *189*, 208–224. https://doi.org/10.1016/j.camwa.2025.04.023

Jafarsadeghi-Pournaki, I., Fakhari, M., Amiri, A., & Rezazadeh, G. (2015). Vibration analysis of circular magneto-electro-elastic nano-plates based on Eringen's nonlocal theory. *International Journal of Engineering*, *28*(12), 1808–1817. https://doi.org/10.5829/idosi.ije.2015.28.12c.15

Jamalpoor, A., Ahmadi-Savadkoohi, A., Hosseini, M., & Hosseini-Hashemi, S. (2017). Free vibration and biaxial buckling analysis of double magneto-electro-elastic nanoplate systems coupled by a visco-Pasternak medium via nonlocal elasticity theory. *European Journal of Mechanics - A/Solids*, *63*, 84–98. https://doi.org/10.1016/j.euromechsol.2016.12.002

Ke, L.-L., Wang, Y.-S., Yang, J., & Kitipornchai, S. (2014). Free vibration of size-dependent magneto-electro-elastic nanoplates based on the nonlocal theory. *Acta Mechanica Sinica*, *30*(4), 516–525. https://doi.org/10.1007/s10409-014-0072-3

Liu, C., Ke, L.-L., Wang, Y.-S., Yang, J., & Kitipornchai, S. (2013). Thermo-electro-mechanical vibration of piezoelectric nanoplates based on the nonlocal theory. *Composite Structures*, *106*, 167–174. https://doi.org/10.1016/j.compstruct.2013.05.031

Malikan, M., & Nguyen, V. B. (2018). Buckling analysis of piezo-magnetoelectric nanoplates in hygrothermal environment based on a novel one variable plate theory combining with higher-order nonlocal strain gradient theory. *Physica E: Low-dimensional Systems and Nanostructures*, *102*, 8–28. https://doi.org/10.1016/j.physe.2018.04.018

Martin, L. W., Crane, S. P., Chu, Y.-H., Holcomb, M. B., Gajek, M., Huijben, M., Yang, C.-H., Balke, N., & Ramesh, R. (2008). Multiferroics and magnetoelectrics: Thin films and nanostructures. *Journal of Physics: Condensed Matter*, *20*(43), 434220. https://doi.org/10.1088/0953-8984/20/43/434220

Mohammadimehr, M., & Rostami, R. (2017). Bending, buckling, and forced vibration analyses of nonlocal nanocomposite microplate using TSDT considering MEE properties dependent to various volume fractions of CoFe2O4-BaTiO3. *Journal of Theoretical and Applied Mechanics*, *55*, 853. https://doi.org/10.15632/jtam-pl.55.3.853

Phung-Van, P., Hung, P., Tangaramvong, S., Nguyen-Xuan, H., & Thai, C. H. (2025). A novel Chebyshev-based both meshfree method and shear deformation theory for functionally graded triply periodic minimal surface flat plates. *Computers & Structures*, *309*, 107660. https://doi.org/10.1016/j.compstruc.2025.107660

Phung-Van, P., Nguyen-Xuan, H., Hung, P., & Thai, C. H. (2024). Nonlinear isogeometric analysis of magneto-electro-elastic porous nanoplates. *Applied Mathematical Modelling*, *128*, 331–346. https://doi.org/10.1016/j.apm.2024.01.025

Reddy, J. N. (1984). A simple higher-order theory for laminated composite plates. *Journal of Applied Mechanics*, *51*(4), 745–752. https://doi.org/10.1115/1.3167719

Thai, C. H., Ferreira, A., Nguyen-Xuan, H., Hung, P., & Phung-Van, P. (2023). A nonlocal strain gradient isogeometric model for free vibration analysis of magneto-electro-elastic functionally graded nanoplates. *Composite Structures*, *316*, 117005. https://doi.org/10.1016/j.compstruct.2023.117005

Thai, C. H., Hung, P., Nguyen-Xuan, H., & Phung-Van, P. (2023). A size-dependent meshfree approach for magneto-electro-elastic functionally graded nanoplates based on nonlocal strain gradient theory. *Engineering Structures*, *292*, 116521. https://doi.org/10.1016/j.engstruct.2023.116521

Thai, C. H., Hung, P., Nguyen-Xuan, H., & Phung-Van, P. (2024). A free vibration analysis of carbon nanotube reinforced magneto-electro-elastic nanoplates using nonlocal strain gradient theory. *Finite Elements in Analysis and Design*, *236*, 104154. https://doi.org/10.1016/j.finel.2024.104154

Thai, C. H., Hung, P., & Phung-Van, P. (2025). Naturally stabilized nodal integration of Chebyshev moving Kriging meshless approach for functionally graded triply periodic minimal surface plates. *Engineering Analysis with Boundary Elements*, *179*, 106333. https://doi.org/10.1016/j.enganabound.2025.106333

Von Hippel, A. (1950). Ferroelectricity, domain structure, and phase transitions of barium titanate. *Reviews of Modern Physics*, *22*(3), 221–237. https://doi.org/10.1103/revmodphys.22.221

Zheng, H., Wang, J., & Lofland, S. E. (2004). Multiferroic BaTiO3-CoFe2O4 nanostructures. *Science*, *303*(5658), 661–663. https://doi.org/10.1126/science.1094207

Zur, K. K., Arefi, M., Kim, J., & Reddy, J. N. (2020). Free vibration and buckling analyses of magneto-electro-elastic FGM nanoplates based on nonlocal modified higher-order sinusoidal shear deformation theory. *Composites Part B: Engineering*, *182*, 107601. https://doi.org/10.1016/j.compositesb.2019.107601